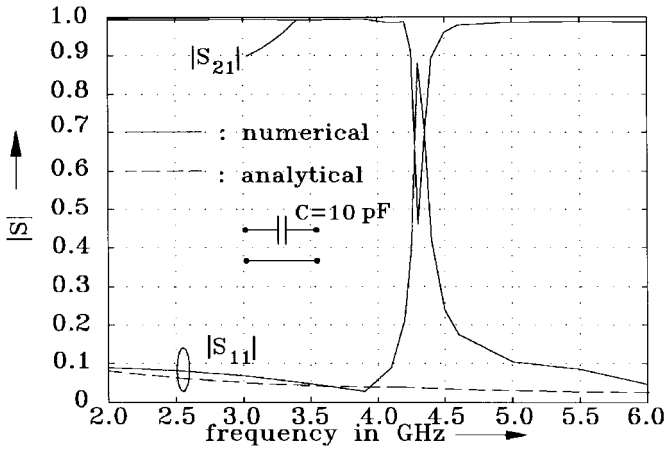

Fig. 7. S-parameters for multilayered capacitor.

An important part of the modeling procedure was the interface of the 3-D model for the SMD's with the surface-current model of the metallizations forming the planar circuit. Using this method, we investigated homogeneous and multilayered SMD capacitors within a microstrip circuit. For the homogeneous capacitor, we could not observe any resonances, although the shortest wavelength in the dielectric was shorter than the length of the capacitor. For the multilayered capacitor with larger capacitances, we found resonances with frequencies dependent on the capacitance values.

REFERENCES

[1] M.-J. Tsai, C. Chen, N. G. Alexopoulos, and T.-S. Horng, "Multiple arbitrary shape via-hole and air-bridge transitions in multilayered structures," *IEEE Trans. Microwave Theory Tech.*, vol. 44, pp. 2504–2511, Dec. 1996.

[2] T. F. Eibert and V. Hansen, "3D FEM/BEM—Hybrid approach for planar layered media," *Electromagn.*, vol. 16, no. 3, pp. 253–272, May/June 1996.

[3] ——, "3-D FEM/BEM—Hybrid approach based on a general formulation of Huygens' principle for planar layered media," *IEEE Trans. Microwave Theory Tech.*, vol. 45, pp. 1105–1112, July 1997.

TM Scattering from Hollow and Dielectric-Filled Semielliptic Channels with Arbitrary Eccentricity in a Perfectly Conducting Plane

W. J. Byun, J. W. Yu, and N. H. Myung

***Abstract*— The behavior of TM wave scattering from hollow and dielectric-filled semielliptic channels in a perfectly conducting substrate is investigated. The scattered field is represented in terms of an infinite series of Mathieu functions with unknown coefficients. By applying the separation of variables and employing the partial orthogonality of the first-kind angular Mathieu functions, the unknown coefficients are obtained. Numerical results are given for the scattered-field patterns by the channels with different eccentricities and permittivities.**

***Index Terms*—Electromagnetic scattering, Mathieu functions, semielliptic channel.**

I. INTRODUCTION

A considerable number of investigations have been performed on the radar cross section (RCS) analysis for the geometries with channels, grooves, and cracks in a perfectly electric conducting (PEC) substrate. This is due to the fact that these local guiding structures may excite internal resonances, and they sometimes yield scattering contribution which cannot be obtained with other ordinary geometries. The electromagnetic scattering effect from a square groove in a PEC substrate has been treated in [1] and a semicircular one treated in [2]–[4]. However, a scattering solution is not available for semielliptic channels in a PEC substrate. In this paper, TM scattering from semielliptic channels is solved with different eccentricities and permittivities in a PEC plane by employing the separation of variables and mode-matching method. In elliptic cylinder coordinates, separation of variables leads to Mathieu's equation, which has solutions in the form of Mathieu functions [5]. Although the familiar orthogonality relationships at the interface cannot be applied for the scattering problem of dielectric-filled geometries, an analytic-series solution to electromagnetic scattering by dielectric-filled semielliptic channels is presented in this paper.

II. FIELD REPRESENTATIONS

The problem is formulated with respect to elliptic cylinder coordinates ζ and η where $x = d, \cosh\zeta, \cos\eta$, $y = d, \sinh\zeta, \sin\eta$, and d is the semifocal distance in Fig. 1. The semielliptic interface between Regions I and II is represented by the relation ζ_0 $(e = 1/\cosh\zeta_0 = d/a)$. The eccentricity e is represented by $\sqrt{1-(b/a)^2}$, and a and b are semimajor and semiminor axis, respectively. The normalization factors adopted by Ince [6] are used, and Mathieu functions are computed using the algorithms in [7]. Throughout this paper, the $e^{j\omega t}$ time–harmonic factor is assumed and suppressed. The TM_z plane wave impinges on a dielectric-filled semielliptic channel in a PEC substrate at the incident angle of ϕ_i with respect to the x-axis, as shown in Fig. 1. The semielliptic channel has a wavenumber $k_1 (= \omega\sqrt{\mu_0\epsilon_0\epsilon_r})$. When the incident wave impinges on the channel in a PEC substrate, a surface scattering

Manuscript received August 1, 1997; revised January 26, 1998.

The authors are with the Department of Electrical Engineering, Korea Advanced Institute of Science and Technology (KAIST), Taejon 305-701, Korea (e-mail: nhmyung@eekaist.kaist.ac.kr; bwj@cais.kaist.ac.kr).

Publisher Item Identifier S 0018-9480(98)06156-0.

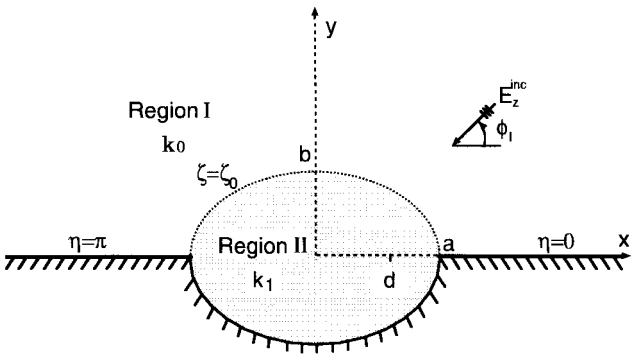

Fig. 1. Geometry of a dielectric-filled semielliptic channel in a PEC substrate.

process takes place, resulting in scattered, specularly reflected, and transmitted fields.

In Region I ($\zeta > \zeta_0,\ 0 < \eta < \pi$), the total field may be decomposed into three parts: the incident, specularly reflected, and scattered fields [8]. The incident and specularly reflected fields are represented by

$$E_z^i(\zeta,\eta) = \sum_{n=1}^{\infty} 2(j)^n Ms_n^{(1)}(\zeta, q_0) se_n(\eta, q_0) se_n(\phi_i, q_0) + \sum_{n=0}^{\infty} 2(j)^n Mc_n^{(1)}(\zeta, q_0) ce_n(\eta, q_0) ce_n(\phi_i, q_0) \quad (1)$$

$$E_z^r(\zeta,\eta) = -E_z^i(\zeta,\eta) \quad \text{with} \quad \phi_i \to 2\pi - \phi_i \quad (2)$$

where $q_i = (k_i ae)^2/4$ for $i = 0, 1$, and k_0 is the wavenumber in free space. The even and odd angular Mathieu functions of order n and the first kind are denoted by $ce_n(\eta, q_i)$ and $se_n(\eta, q_i)$, respectively. $Mc_n^{(s)}(\zeta, q_i)$, $Ms_n^{(s)}(\zeta, q_i)$ for $s = 1$ and 2 are the even and odd radial Mathieu functions of the sth kind. The scattered field in Region I may be given by imposing boundary condition $E_z^s = 0$ on the PEC substrate since $se_n(\eta, q_0) = 0$ at $\eta = 0$ and π, and it is represented by

$$E_z^s(\zeta,\eta) = \sum_{n=1}^{\infty} A_n Ms_n^{(4)}(\zeta, q_0) se_n(\eta, q_0) \quad (3)$$

where $Ms_n^{(4)}(\zeta, q_0)$ is the Mathieu function which corresponds to the Hankel function of the second kind in circular cylindrical coordinates and has the relationship of $Ms_n^{(4)}(\zeta, q_0) = Ms_n^{(1)}(\zeta, q_0) - jMs_n^{(2)}(\zeta, q_0)$. Then, the total field in Region I is represented by

$$\begin{aligned} E_z^I(\zeta,\eta) &= E_z^i(\zeta,\eta) + E_z^r(\zeta,\eta) + E_z^s(\zeta,\eta) \\ &= \sum_{n=1}^{\infty} 4(j)^n Ms_n^{(1)}(\zeta, q_0) se_n(\eta, q_0) se_n(\phi_i, q_0) \\ &\quad + \sum_{n=1}^{\infty} A_n Ms_n^{(4)}(\zeta, q_0) se_n(\eta, q_0). \end{aligned} \quad (4)$$

In Region II ($\zeta < \zeta_0,\ 0 < \eta < 2\pi$), the transmitted electric field may also be represented as

$$E_z^{II}(\zeta,\eta) = \sum_{n=0}^{\infty} B_n Mc_n^{(1)}(\zeta, q_1) ce_n(\eta, q_1) + \sum_{n=1}^{\infty} C_n Ms_n^{(1)}(\zeta, q_1) se_n(\eta, q_1). \quad (5)$$

From Maxwell's equations, the η-components of the magnetic field may be represented as

$$H_\eta^{I(II)}(\zeta,\eta) = -\frac{j}{\omega\mu_0 L}\frac{\partial E_z^{I(II)}}{\partial \zeta} \quad (6)$$

where $L = d\sqrt{\cosh^2\zeta - \cos^2\eta}$. In (3)–(5), A_n, B_n, and C_n are unknown coefficients to be determined with the boundary conditions at $\zeta = \zeta_0$ of zero tangential electric field on the channel ($\pi < \eta < 2\pi$) and field continuity across the aperture ($0 < \eta < \pi$). Applying the orthogonality condition of the angular Mathieu functions and eliminating C_n, the simultaneous equations, shown in (7)–(14), at the bottom of this page, can be obtained in terms of A_n and B_n for $m \geq 1$, where $p = 1, 4$. The prime in the above equations denotes the derivative with respect to ζ. In the case of a hollow channel,

$$\sum_{n=0}^{\infty} B_n Vc_{mn}^{(1)}(\zeta_0, q_1) X_{mn} - \sum_{n=1}^{\infty} A_n Vs_{mn}^{(4)}(\zeta_0, q_0) Z_{mn} = \sum_{n=1}^{\infty} 4(j)^n Vs_{mn}^{(1)}(\zeta_0, q_0) se_n(\phi_i, q_0) Z_{mn} \quad (7)$$

$$\sum_{n=0}^{\infty} B_n \left\{ Uc_{mn}^{(1)}(\zeta_0, q_1) X_{mn} - Mc_n^{(1)}(\zeta_0, q_1) Y_{mn} \right\} - \sum_{n=1}^{\infty} A_n Us_{mn}^{(4)}(\zeta_0, q_0) Z_{mn} = \sum_{n=1}^{\infty} 4(j)^n Us_{mn}^{(1)}(\zeta_0, q_0) se_n(\phi_i, q_0) Z_{mn} \quad (8)$$

$$Us, c_{mn}^{(p)}(\zeta_0, q_{0,1}) = \frac{Ms_m^{(1)}(\zeta_0, q_1)}{Ms_m^{(1)\prime}(\zeta_0, q_1)} Ms, c_n^{(p)\prime}(\zeta_0, q_{0,1}) \quad (9)$$

$$Vs, c_{mn}^{(p)}(\zeta_0, q_{0,1}) = Ms, c_n^{(p)}(\zeta_0, q_{0,1}) - Us, c_{mn}^{(p)}(\zeta_0, q_{0,1}) \quad (10)$$

$$C_m Ms_m^{(1)\prime}\frac{\pi}{2}\delta_{mn} = \sum_{n=1}^{\infty} \left\{ A_n Ms_n^{(4)\prime}(\zeta_0, q_0) + 4(j)^n Ms_n^{(1)\prime}(\zeta_0, q_0) se_n(\phi_i, q_0) \right\} Z_{mn} - \sum_{n=0}^{\infty} B_n Mc_n^{(1)\prime}(\zeta_0, q_1) X_{mn} \quad (11)$$

$$X_{mn} = \int_0^{\pi} ce_n(\eta, q_1) se_m(\eta, q_1)\, d\eta \quad (12)$$

$$Y_{mn} = \int_{\pi}^{2\pi} ce_n(\eta, q_1) se_m(\eta, q_1)\, d\eta = -X_{mn} \quad (13)$$

$$Z_{mn} = \int_0^{\pi} se_n(\eta, q_0) se_m(\eta, q_1)\, d\eta \quad (14)$$

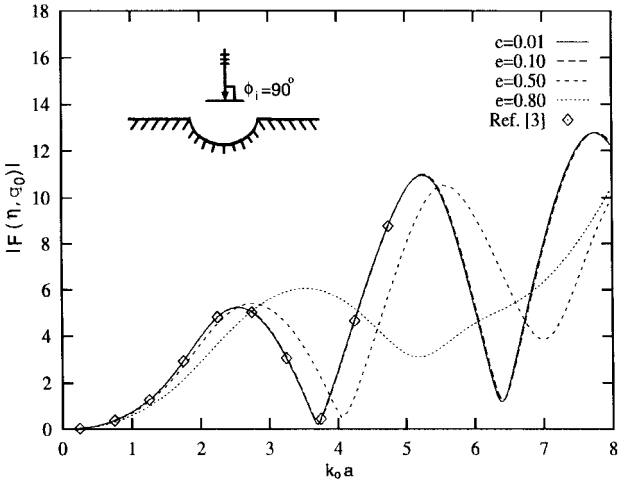

Fig. 2. Normalized backscattered field versus k_0a for a hollow semielliptic channel ($k_1 = k_0$, $\phi_i = \eta = 90°$).

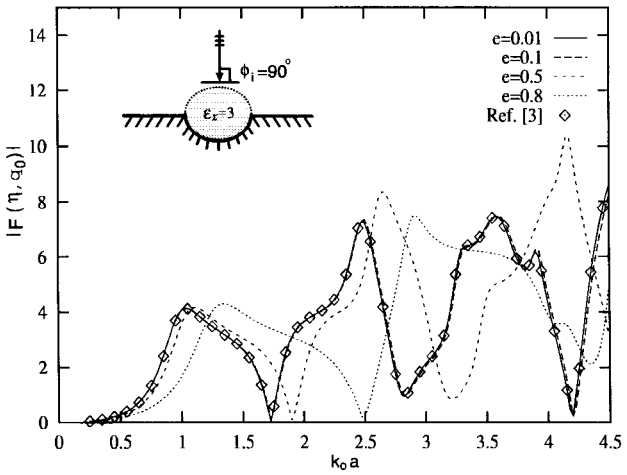

Fig. 3. Normalized backscattered field versus k_0a for a dielectric-filled channel ($\epsilon_r = 3$, $\phi_i = \eta = 90°$).

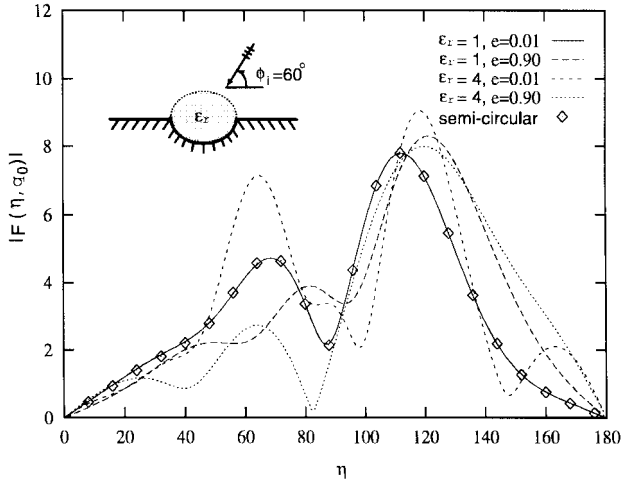

Fig. 4. Scattered field versus scattering angle η for a semielliptic channel ($k_0a = 2\pi$, $\phi_i = 60°$).

$q_1 = q_0$ and $Z_{mn} = (\pi/2)\delta_{mn}$, where δ_{mn} is the Kronecker delta, and (7) and (8) can be reduced to

$$\sum_{n=0}^{\infty} B_n W_{mn}(\zeta_0, q_0) X_{mn} = 2\pi(j)^m Q_{mn}(\zeta_0, q_0) se_m(\phi_i, q_0)\,\delta_{mn} \tag{15}$$

$$A_m \frac{\pi}{2} V s_{mn}^{(4)}(\zeta_0, q_0)\,\delta_{mn} = \sum_{n=0}^{\infty} B_n V c_{mn}^{(1)}(\zeta_0, q_0) X_{mn} - 2\pi(j)^m V s_{mn}^{(1)}(\zeta_0, q_0) se_m(\phi_i, q_0)\,\delta_{mn} \tag{16}$$

$$W_{mn}(\zeta_0, q_0) = M c_n^{(1)}(\zeta_0, q_0) + U c_{mn}^{(1)}(\zeta_0, q_0) - \frac{U s_{mm}^{(4)}(\zeta_0, q_0)}{V s_{mm}^{(4)}(\zeta_0, q_0)} V c_{mn}^{(1)}(\zeta_0, q_0) \tag{17}$$

$$Q_{mn}(\zeta_0, q_0) = U s_{mn}^{(1)}(\zeta_0, q_0) - \frac{U s_{mn}^{(4)}(\zeta_0, q_0)}{V s_{mn}^{(4)}(\zeta_0, q_0)} V s_{mn}^{(1)}(\zeta_0, q_0). \tag{18}$$

The infinite series involved in the solution are convergent, and this makes it possible to truncate after a certain number of terms to determine the unknown coefficients A_n, B_n, and C_n.

III. Field Computation

To check the accuracy and convergence of the formulation developed in this paper, the numerical results of the normalized scattered-field magnitude $|F(\eta, q_0)|$ are calculated and compared with those of a semicircular channel [3]. The formulations for the scattered far field as a function of η are given by [9]

$$M s_n^{(4)} \overset{\zeta \to \infty}{\simeq} \sqrt{\frac{2}{\pi k_0 d \sinh\zeta}}\, e^{-j(k_0 d \sinh\zeta - ((2n+1)\pi/4))} \tag{19}$$

$$d\sinh\zeta \overset{\zeta \to \infty}{\simeq} \rho$$

$$E_z^s(\zeta, \eta) \overset{\zeta \to \infty}{\simeq} \sqrt{\frac{2}{\pi k_0 \rho}}\, e^{-j(k_0\rho - (\pi/4))} F(\eta, q_0) \tag{20}$$

$$F(\eta, q_0) = \sum_{n=1}^{N} (j)^n A_n se_n(\eta, q_0).$$

A plot of the normalized scattered-field magnitude $|F(\eta, q_0)|$ versus k_0a for a hollow channel at normal incidence is shown in Fig. 2 for four different eccentricities. As one can see from Fig. 2, the scattered field for the $e = 0.01$ case agrees well with that of a semicircular channel, which can be considered as the limiting geometry of the semielliptic one. Although the scattered field for the different eccentricities shows similar patterns, k_0a for maximum and minimum points of scattered-field magnitude increases as the eccentricity increases. This implies that k_0a, which corresponds to the cutoff wavenumber of the elliptic waveguide, increases as eccentricity increases [10]. Fig. 3 shows the behavior of $|F(\eta, q_0)|$ versus k_0a for the four different eccentricities with normal incidence and $\varepsilon_r = 3$. From Fig. 3, it is seen that a presence of the dielectric loading tends to decrease the period of the resonance versus k_0a. The effect of increasing the eccentricity is the same as that of Fig. 2. In Fig. 4, $|F(\eta, q_0)|$ is plotted versus the scattering angle η with $\phi_i = 60°$, $k_0a = 2\pi$, and $\varepsilon_r = 1, 4$. It is noted that the main lobes exist at the forward directions and their magnitudes and directions depend on eccentricities. It is also worth noting that $A_n = B_n = 0$ from (15) and (16) since $Ms_n^{(1)}(0, q_0) = Q_{mn}(0, q_0) = Vs_{mn}^{(1)}(0, q_0) = 0$ from (9), (10), and (18) in the case of $e = 1 (\epsilon_r = 1)$. Therefore, the simple reflection of a plane wave incident on the PEC infinite plane is obtained from (4). In Fig. 5(a), the behavior of $|E_z(\zeta, \eta)|$ in the neighborhood of the hollow channel is plotted for $\phi_i = 90°$, $\epsilon_r = 1$, $e = 0.5$, and $k_0a = 4.28$ corresponding to the cutoff wavenumber of the odd TM_{11} mode [10], [11]. The same plot is repeated in

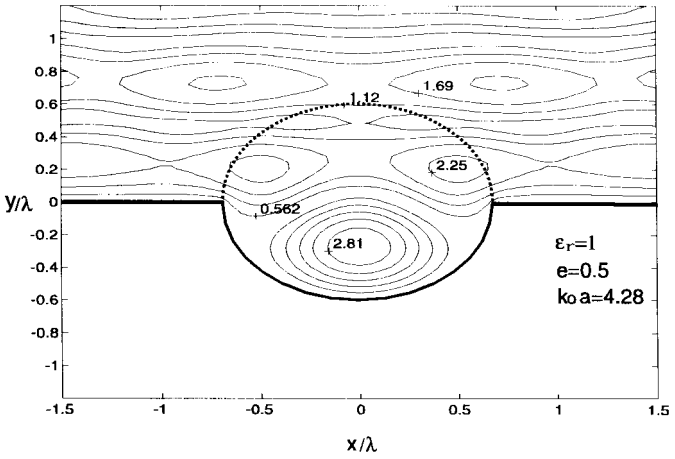

(a)

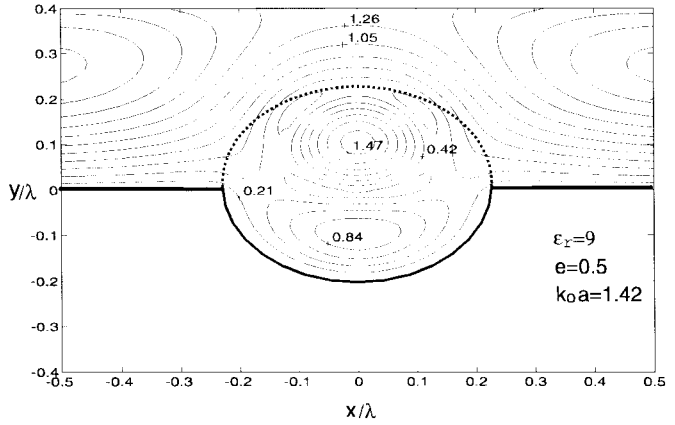

(b)

Fig. 5. Equiamplitude contour plots of $|E_z(\zeta, \eta)|$ near: (a) a hollow semielliptic channel ($k_0a = 4.28$, $\epsilon_r = 1$, $e = 0.5$, $\phi_i = 90^\circ$) and (b) a dielectric-filled channel ($k_0a = 1.42$, $\epsilon_r = 9$, $e = 0.5$, $\phi_i = 90^\circ$).

Fig. 5(b) for $\phi_i = 90^\circ$, $\epsilon_r = 9$, $e = 0.5$, and $k_0a = 1.42$. The field pattern inside the channel is similar to the odd TM_{11} mode. From Fig. 5(a) and (b), it is seen that the boundary condition on the conducting plane is satisfied.

IV. Conclusion

An analytic-series solution based on the mode-matching method for hollow and dielectric-filled semielliptic channels is introduced in this paper. The validity and accuracy of the numerical results are examined by comparing the scattered-field pattern with those of the semicircular channels, which can be considered as the limiting geometry of the semielliptic one. The resonances in surface scattering with the semielliptic channels are seen to depend not only on the size of the channel and permittivity of the dielectric loading, but on the eccentricity. In addition, the scattered-field pattern depends very much on the eccentricity of the semielliptic channels.

References

[1] T. B. A. Senior and J. L. Volakis, "Scattering by gaps and cracks," *IEEE Trans. Antennas Propagat.*, vol. 37, pp. 744–750, June 1989.

[2] M. Hinders and A. Yaghjian, "Dual series solution to scattering from a semicircular channels in a ground plane," *IEEE Trans. Microwave Guided Wave Lett.*, vol. 1, pp. 239–242, Sept. 1991.

[3] T. J. Park, H. J. Eom, W. M. Boerner, and Y. Yamaguchi, "TM scattering from a dieletric-loaded semi-circular trough in a conducting plane," *IEICE Trans. Commun.*, vol. E75-B, no. 2, pp. 87–91, Feb. 1992.

[4] R. A. Ragheb, "Electromagnetic scattering from a coaxial dielectric circular cylinder loading a semicircular gap in a ground plane," *IEEE Trans. Microwave Theory Tech.*, vol. 43, pp. 1303–1309, June 1995.

[5] N. W. McLachlan, *Theory and Applications of Mathieu Functions.* New York: Dover, 1964.

[6] A. N. Lowan, *et al.*, *Tables Relating to Mathieu Functions: Characteristic Values, Coefficients, and Joining Factors* (NBS Appl. Math. Series 59). New York: Dover, 1967.

[7] D. S. Clemm, "Characteristic values and associated solutions of Mathieu's differential equations $[S_{22}]$," *Commun. ACM*, vol. 12, no. 7, pp. 399–408, July 1969.

[8] J. W. Yu and N. H. Myung, "TM scattering by a wedge with concaved edge," *IEEE Trans. Antennas Propagat.*, vol. 45, pp. 1315–1316, Aug. 1997.

[9] T. Hinata, H. Hosono, and H. Ono, "Scattering of electromagnetic waves by an axially slotted conducting elliptic cylinder," *IEICE Trans. Electron.*, vol. E79-C, no. 10, pp. 1364–1370, Oct. 1996.

[10] S. Zhang and Y. Shen, "Eigenmode sequence for an elliptic waveguide with arbitrary ellipticity," *IEEE Trans. Microwave Theory Tech.*, vol. 43, pp. 227–230, Jan. 1995.

[11] B. K. Wang, K. Y. Lam, M. S. Leong, and P. S. Kooi, "Elliptical waveguide analysis using improved polynomial approximation," *Proc. Inst. Elect. Eng.*, vol. 141, no. 6, pp. 483–488, Dec. 1994.

Efficient Parameter Computation of 2-D Multiconductor Interconnection Lines in Layered Media by Convergence Acceleration of Dielectric Green's Function via Padé Approximation

Ji Zheng and Zhengfan Li

***Abstract*—In this paper, a novel method is presented for calculation of the capacitance matrix of two-dimensional (2-D) interconnection lines embedded in layered dielectric media. In this method, Padé approximation is used to accelerate the convergence of Green's function, which leads to obvious improvements of computational efficiency for interconnect parameters. The obtained results show good agreement with those in previous publications.**

***Index Terms*—Capacitance, Green's function, interconnections.**

I. Introduction

Today, with increasing integration scale and clock frequency, the major limiting factors for further increasing the operating speed of integrated circuits (IC's) are interconnection delay and crosstalk, rather than the device switching speed. Parameter extraction for interconnects is a key step in the analysis of such delay and crosstalk

Manuscript received October 4, 1996; revised December 5, 1997. This work was supported by the National Natural Science Foundation of China.

J. Zheng was with the Department of Electronic Engineering, Shanghai Jiao Tong University, Shanghai 200052, China. He is now with the Department of Electrical and Computer Engineering, Oregon State University, Corvallis, OR 97331-3211 USA.

Z. Li is with the Department of Electronic Engineering, Shanghai Jiao Tong University, Shanghai 200052, China.

Publisher Item Identifier S 0018-9480(98)06157-2.